

Numerical study of highly birefringent multi-core photonic crystal fiber sensor based on surface plasmon resonance

JIAN-FEI LIAO^{a,b,*}, ZI-PING DING^b, TIAN-YE HUANG^c, YING-MAO XIE^b, ZE-KAI ZENG^b, RUI-QI ZENG^b

^a*School of Mechanical and Electrical Engineering, Wuyi University, Wuyishan 354300, China*

^b*College of Physics and Electronic Information, Gannan Normal University, Ganzhou 341000, China*

^c*School of Mechanical Engineering and Electronic Information, China University of Geosciences (Wuhan), 430074, Wuhan, China*

Based on the surface plasmon resonance effect, a new type of near-infrared multi-core photonic crystal fiber sensor with one analyte channel is proposed. The proposed sensor can effectively eliminate the interference between neighboring analyte channels and improve its signal-to-noise ratio thanks to its single analyte channel structure. The sensing performance is theoretically studied through using the full-vector finite method. Numerical results indicate that, the thickness of the indium tin oxide film has a large influence on the resonance wavelength and the peak of loss while the effect of elliptical air hole size on the property of the proposed sensor is so small. Furthermore, the wavelength sensitivity is 4,400 nm/refractive index unit and the resolution is up to 2.27×10^{-6} . Benefitting from its excellent sensing performance, the proposed sensor can be applied in environmental, food safety and (bio)chemical detection.

(Received September 8, 2020; accepted October 7, 2021)

Keywords: Photonic crystal fiber, Surface plasmon resonance, Sensor, Birefringence

1. Introduction

Surface plasmon resonance (SPR) is usually defined as a charge density oscillation at the interface of metal and dielectric. The principle of SPR is that, when a beam of light is incident to the interface of two materials with permittivity of opposite signs, a collective electronic oscillation happens and leads to stimulate surface plasmon wave (SPW). In this situation, when the incident wave frequency is equal to the electronic oscillation frequency, the most of the optical wave energy is coupled to surface plasmon polaritons (SPP), and then SPR occurs [1]. Benefitting from its extremely sensitivity to the refractive index of the ambient dielectric medium, SPR is regarded as one of the promising technologies in biochemical and attracted more and more attention. SPR sensor is usually realized with a prism deposited a layer of metal materials including silver and gold. Nevertheless, prism-based SPR sensors are not appropriate for some applications such as safety control in danger area. For the purpose of overcoming this drawback, photonic crystal fiber (PCF) is used to displace the prism for designing SPR-based sensor [2-5]. Compared to these prism-based SPR sensors, SPR-based PCF sensors have several advantages such as low cost, label-free sensing, spatial miniaturization, higher sensing performance, *etc* [6-9]. Hence, SPR-based PCF sensors have been extensively investigated all over the world in recent year [10-12].

As we know, the sensing property of PCF-based SPR sensor is relation to fiber structure, parameters, the characteristic of coated metal material, etc. Nowadays,

various of SPR-based PCF sensors with different fiber design have been proposed [13,14]. For instance, hexagonal lattice PCF SPR sensors [15, 16], D-Shaped PCF SPR sensors [17, 18], slotted PCF SPR sensors [19-21], and so on. For the purpose of improving the sensing performance, Paul proposed a new type of plasmonic refractive index (RI) sensor based on an octagonal PCF for monitoring of transformer oil [22]. The simulation results show that the maximum amplitude sensitivity of the *x*- and *y*-polarized modes can be up to 31,240 RIU⁻¹ and 30,830 RIU⁻¹, respectively. Moreover, the figure of merit of the proposed sensor is as high as 5,000. With the aim of realizing high refractive index sensing, Paul et al. proposed another type of plasmonic sensor based on an air-core PCF [23]. The results find that the wavelength sensitivity and resolution of the proposed sensor are as high as 11,700 nm/RIU and 8.55×10^{-6} RIU, respectively. Similarly, Rahman et al. reported a highly sensitive gold-coated PCF based plasmonic RI sensor with a maximum wavelength and amplitude sensitivity of 13,000 nm/RIU and 953.23 RIU⁻¹, respectively [1]. Furthermore, Ahmed et al. suggested a dual-core PCF based SPR sensor where the maximum wavelength sensitivity, resolution and amplitude sensitivity are 16,000 nm/RIU, 6.25×10^{-6} RIU and 2255 RIU⁻¹, respectively [24]. However, most of PCF-based SPR sensors usually employ silver or gold, which leads to high sensing cost. Moreover, these noble metals also makes most of SPR-based PCF sensors work in the visible waveband, and then deteriorates the sensing performance for large-scale targets detection such as cells or proteins since the penetration depth of the evanescent

field is in proportion to the working wavelength. Recently, indium tin oxide (ITO) has attracted much more interests for plasmonic application because of its several advantages [14, 25]. First of all, the carrier density of ITO can be changed by electrical gating, highly doping with aluminum, and post-deposition rapid thermal annealing processes [26, 27]. This property supplies an effectively method to modify the complex refractive index of ITO material. Secondly, ITO material has not band to band conversion, and then the island formation can not be formed in ITO material [28]. Finally, it is well known that ITO material is much cheaper than silver and gold. Hence, ITO provides a cost-effective way to constitute PCF-based SPR sensor at the near-infrared region.

In this paper, utilizing the above merits of ITO, a new type of highly birefringent multi-core PCF sensor based on SPR by employing ITO as the plasmon active metal material is proposed. The effects of fiber parameters on sensing characteristic are theoretical investigated. The results demonstrate that the resonance wavelength and the peak of loss of our proposed sensor can be modified simply through adjusting the thickness of ITO film. On the other hand, the elliptical air hole size has a very small impact on the sensor's property. Finally, benefitting from its single analyte channel design, the proposed sensor has only one resonance wavelength within the simulation wavelength range, and this property can effectively improve the sensor's signal-to-noise ratio.

2. Sensor design

Fig. 1 gives the schematic of our designed SPR-based PCF sensor. There is four layers of elliptical air-holes located in PCF cladding, and these holes are arranged in a triangular lattice. The six cores are constructed by substituting six silica rods with six elliptical holes in the second layer, and are named by employing the numbers 1-6. The light wave in each individual fiber core follows total internal reflection principle. Moreover, there is only one circle analyte channel located in the center of fiber core region to improve the sensor's signal-to-noise ratio. The sensor structure is arranged in such a manner that the incident light can run away from the fiber core region to the ITO-silica interface. The escape photon energy can stimulate the oscillating electronics of ITO film, which leads to the generation of SPW. The proposed sensor is characterized by the pitch Λ , the lengths of elliptical holes along the minor axis a and the major axis b , the thickness of ITO film t , the diameter of the central circle analyte channel D . The substrate of the sensor is silica, and its refractive index is calculated from the Sellmeier equation [29]. The permittivity of ITO is determined by the Drude-Lorentz model. [30]

$$\varepsilon = \varepsilon_{\infty} - \omega_p^2 / (\omega^2 + i\omega\Gamma) \quad (1)$$

$$\omega_p^2 = ne^2 / (\varepsilon_{\infty} m^*) \quad (2)$$

where ε = the permittivity of ITO, $\varepsilon_{\infty} = 3.9$ is the high frequency permittivity, ω = angular frequency, ω_p = plasma frequency, $\Gamma = 1.8 \times 10^{14} \text{ rad/s}$ is the electron scattering rate, $m^* = 0.35m_0$, $m_0 = 9.1 \times 10^{-31} \text{ kg}$ is the rest mass of electrons, $n = 1.8 \times 10^{21} \text{ cm}^{-3}$ is the carrier concentration of ITO, e = electron charge. Compared to other PCF based SPR sensors coated with graphene/gold/silver, our proposed SPR sensor has the following advantages. Firstly, ITO material is much cheaper and leads to low cost. Secondly, single analyte channel structure can efficiently remove the disturbance between adjacent analyte channels. Thirdly, high birefringent sensor design can efficiently eliminate the crossing interference between these two fundamental polarized modes.

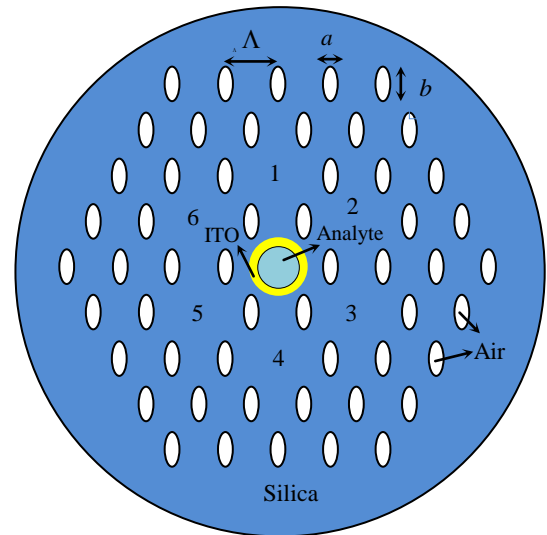


Fig. 1. The schematic of proposed SPR-based PCF sensor (color online)

3. Simulation results and discussion

For the purpose of studying the modal property precisely, full vector finite element method is adopted with 53432 triangular elements over the whole PCF cross-section. Moreover, the edge and vertex elements are 2892 and 272, respectively. The inter-layer boundary condition applied for other boundaries is continuous boundary conditions while the PML boundary condition is applied at the outermost layer. The simulation results indicate that the x-polarized core mode can't effectively couple with the SPP mode. Therefore, we only investigate the coupling resonance properties between the SPP mode and the y-polarized core mode in this paper.

First of all, we study the birefringent property of our proposed sensor, and the simulation results are shown in Fig. 2. It can be found that the birefringence of our proposed sensor within the wavelength range of 1.3~1.43 μm increases gradually with the wavelength increasing

when b keeps unchanged. However, the birefringence begins to decrease when the wavelength increases from $1.43 \mu\text{m}$ to the resonance wavelength. The reason is that the x - and y -polarized modes can be well confined in the fiber core region in the wavelength range of $1.3 \sim 1.43 \mu\text{m}$ because both of two polarized modes can't effectively couple with the SPP mode. When the wavelength lies in the wavelength range of $1.43 \mu\text{m}$ to the resonance wavelength, most of the energy of the y -polarized mode is coupled into the SPP mode while the x -polarized mode is still confined in the fiber core region, and then the refractive index of the y -polarized mode decreases faster than that of the x -polarized mode. After the coupled resonance point, the birefringence suddenly increases since the refractive index of the y -polarized mode suddenly increases too. This similar phenomenon can be found in other birefringent PCF SPR sensor [21]. Moreover, the birefringence in the whole simulation wavelength range increases significantly when b increases from 1.3 to $1.6 \mu\text{m}$. This is because the structure of the sensor becomes more non-symmetrical when b increases.

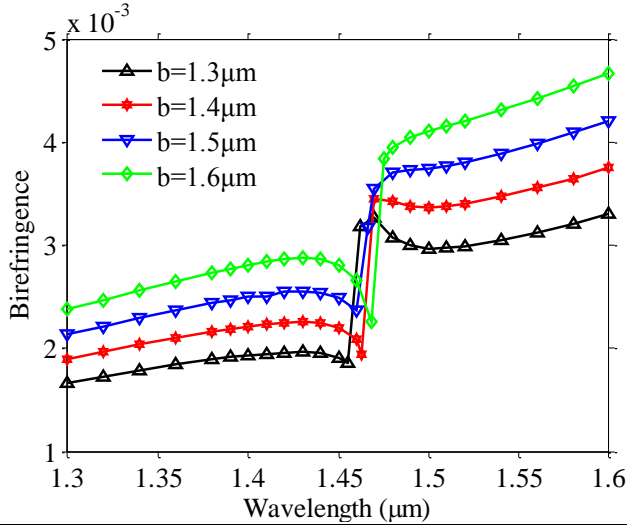


Fig. 2. Birefringent property of the proposed sensor for b changing from 1.3 to $1.6 \mu\text{m}$ (color online)

Secondly, the coupling resonance property of our proposed sensor is investigated. The loss of the sensor is calculated through adopting the equation $\alpha(\text{dB/cm}) = 8.686 \times (2\pi/\lambda) \text{Im}(n_{\text{eff}}) \times 10^4$ [31]. The dispersion relations of the SPP mode and y -polarized core mode are given in Fig. 3 with $\Lambda = 1.8 \mu\text{m}$, $a = 0.6 \mu\text{m}$, $b = 1.4 \mu\text{m}$, $d_c = 0.86 \mu\text{m}$, $t = 60 \text{ nm}$, and the analyte refractive index $n_a = 1.41$. It is apparent from Fig. 3(a) that the real part of the mode effective refractive index of SPP mode ($\text{Re}(n_{\text{spp}})$) is much larger than that of y -polarized core mode ($\text{Re}(n_y)$) within the shorter wavelength range. Nevertheless, with the increment of the wavelength, the difference between $\text{Re}(n_{\text{spp}})$ and $\text{Re}(n_y)$

decreases gradually since $\text{Re}(n_y)$ decreases much slower than $\text{Re}(n_{\text{spp}})$. When the wavelength increases to $1.463 \mu\text{m}$, $\text{Re}(n_y)$ is equivalent to that of the SPP mode, which means that the resonance condition between these two modes is satisfied at the wavelength of $1.463 \mu\text{m}$. The reason is that the phase of the electromagnetic field is affected by the SPR [32]. Further increasing the wavelength, the difference between $\text{Re}(n_{\text{spp}})$ and $\text{Re}(n_y)$ becomes large and the y -polarized mode can't interact efficiently with the SPP mode. The coupling resonance characteristics can also be observed from the inset in Fig. 3(a).

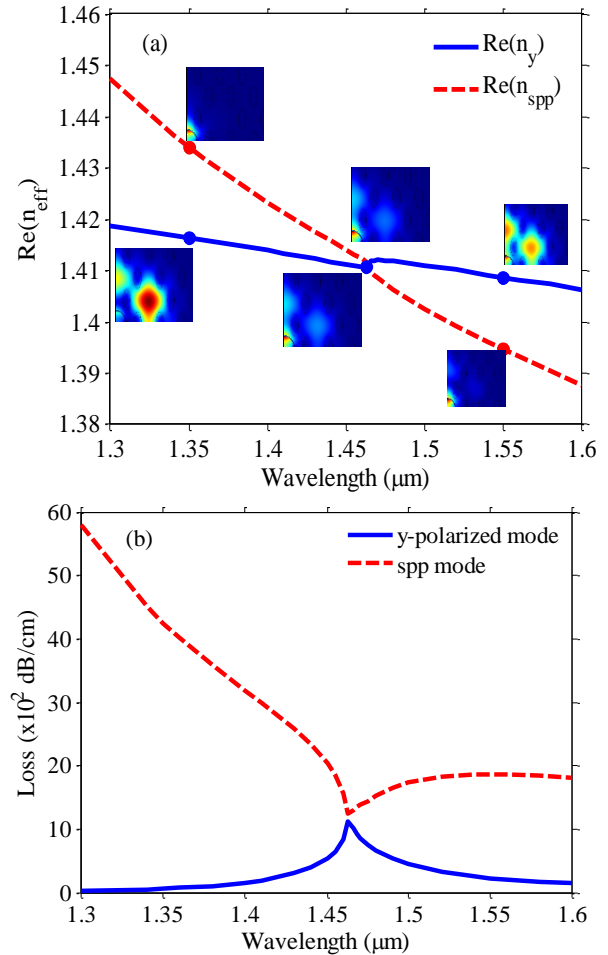


Fig. 3. The real parts of the effective indices (a) and modal loss (b) as a function of wavelength for the proposed PCF SPR sensor. Insets are the mode field distributions of the SPP and y -polarized core modes at different wavelengths (color online)

For instance, the y -polarized core mode at $\lambda = 1.35 \mu\text{m}$ almost can't interact with the SPP mode since the coupling resonance condition between these two modes is not fulfilled. Therefore, the electric field energy of fiber core mode is well confined in the core region while the energy of the SPP mode is well confined at the surface of the ITO layer. However, the mode field distributions of the SPP and fiber core modes are almost the same when λ increases to $1.463 \mu\text{m}$. This is because the coupling

resonance condition between these two modes is satisfied, and then the electric field energy of the core mode is almost conversion into the SPP mode. Further increasing λ to $1.55\mu\text{m}$, the mode field profiles of these two modes are different because the coupling resonance condition is unfulfilled. Fig. 3(b) gives the modal loss property of the SPP and y-polarized core modes. It is apparent from this figure that the loss of the SPP in $1.3\sim 1.6\mu\text{m}$ region is larger than that of the fiber core mode. But the loss of the SPP mode at the resonance wavelength is almost equal to that of the fiber core mode because of the coupling interaction between these two modes. In addition, there is only one loss peak in $1.3\sim 1.6\mu\text{m}$ region thanks to the single circle analyte channel structure. Hence, our proposed sensor has a low signal-to-noise ratio.

Fig. 4 gives the influence of t on the resonance wavelength with $A=1.8\mu\text{m}$, $a=0.6\mu\text{m}$, $b=1.4\mu\text{m}$, $d_c=0.86\mu\text{m}$, and $n_a=1.41$. One can observe that the resonance wavelength moves to longer wavelength when t increases from 55 nm to 75 nm . For instance, the resonance wavelength is around $1.427\mu\text{m}$ when $t=55\text{ nm}$. But if t increases to 75 nm , the resonance wavelength increases to $1.557\mu\text{m}$. The main reason is that $\text{Re}(n_{\text{spp}})$ increases with t increasing while $\text{Re}(n_y)$ almost keeps unchanged. Therefore, the coupling resonance wavelength shifts to the longer wavelength. Moreover, we can also find that the loss of the y-polarized core mode decreases gradually when t increases to 75 nm . This is because the evanescent wave becomes more difficult to penetrate the ITO film when t increases, which leads the coupling interaction between the evanescent wave and SPP mode becoming weaker. Under this situation, the oscillating electronics of ITO film absorb less energy from the y-polarized core mode, and then the loss peak of the y-polarized core mode decreases.

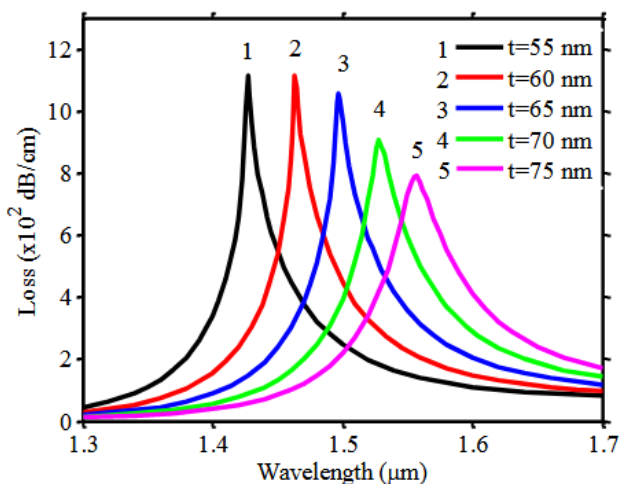


Fig. 4. Influence of the thickness of the ITO layer on the loss (color online)

The influences of fiber parameters a and b on the resonance wavelength are given in Fig. 5. It is apparent

from Fig. 5(a) that a has merely a small effect on the resonance wavelength with $A=1.8\mu\text{m}$, $b=1.4\mu\text{m}$, $d_c=0.86\mu\text{m}$, and $n_a=1.41$. This is because the effect of a on $\text{Re}(n_{\text{spp}})$ and $\text{Re}(n_y)$ is really small, and then the phase matching condition between these two modes almost keeps unchanged. As shown in Fig. 5(b), the influence of b on the resonance wavelength is also small with the fiber parameters of $A=1.8\mu\text{m}$, $a=0.6\mu\text{m}$, $d_c=0.86\mu\text{m}$, and $n_a=1.41$. Therefore, the resonance wavelength of our proposed sensor is insensitive to the variations of a and b . This property will enhance the tolerance on the sensor drawing defects and fluctuations. In addition, the loss peak of the y-polarized core mode decreases gradually when a and b increase. The main reason is that the air-filling factor of the sensor increases with the increment of a and b , which leads to the improvement of the confinement ability of the guided mode. Therefore, the leakage energy of the y-polarized core mode is reduced.

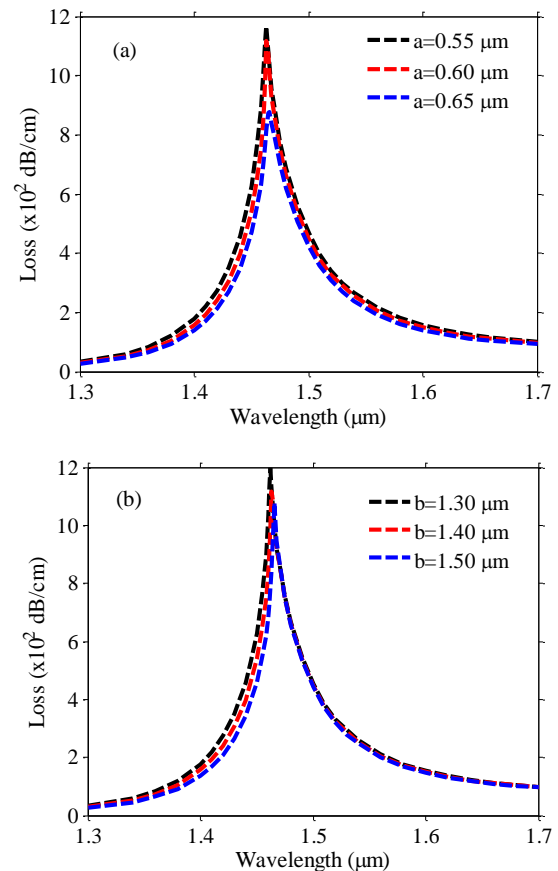


Fig. 5. Influences of fiber parameters a (a) and b (b) on the loss (color online)

For the purpose of further studying the sensing property, we investigate the effect of n_a on the resonance wavelength with parameters of $A=1.8\mu\text{m}$, $a=0.6\mu\text{m}$, $b=1.4\mu\text{m}$, and $d_c=0.86\mu\text{m}$. It is apparent from Fig. 6(a) that the resonance wavelength increases with the analyte refractive index increasing. For example, the resonance

wavelength increases from 1.298 μm to 1.463 μm when n_a increases from 1.36 to 1.41. The main reason is that n_a has a large effect on $\text{Re}(n_{\text{spp}})$ while it has a small effect on $\text{Re}(n_y)$. Therefore, the phase matching point moves to the longer wavelength region. Furthermore, one can find that the loss peak at the resonance wavelength increases quickly when n_a increases from 1.36 to 1.41.

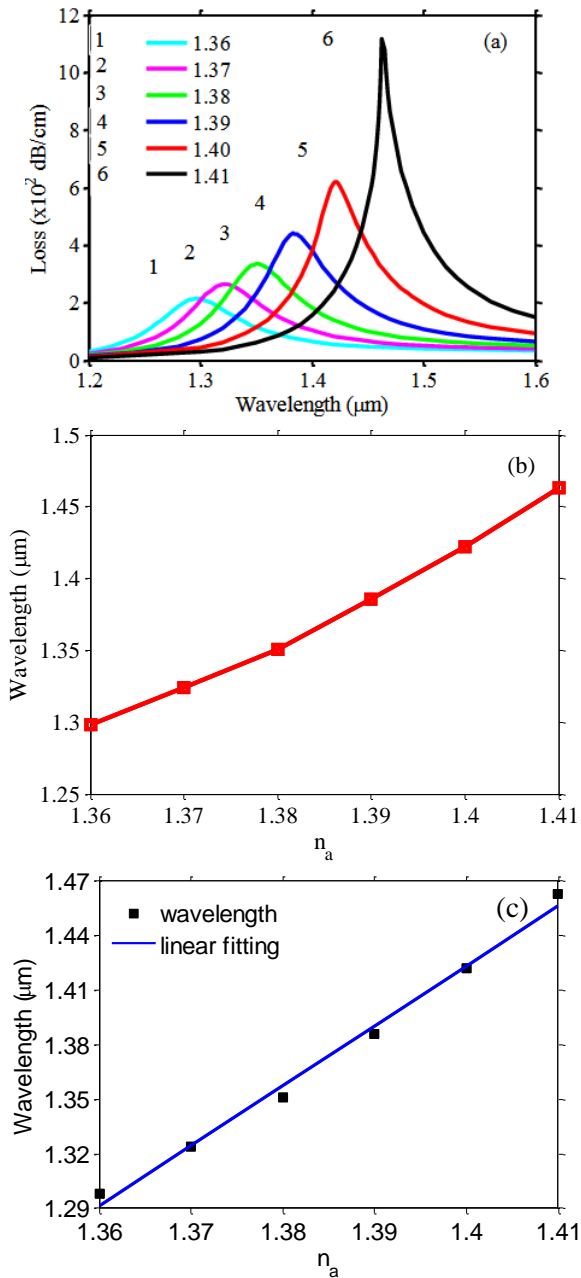


Fig. 6. Loss spectra (a), resonant wavelength, and linear fitting line of the resonance wavelength (c) by varying n_a from 1.36 to 1.41 (color online)

Such as the loss peak is only 214.3 dB/cm when $n_a = 1.36$. But if n_a increases to 1.41, the loss peak is up to 1,115 dB/cm. This is because the coupling strength between these two modes is enhanced when n_a increases. Therefore, more electric field energy of the fiber core mode is conversion into the SPP mode. The resonance wavelength at different analyte refractive index is given in Fig. 6(b). For the purpose of calculating the wavelength sensitivity, the equation $S_\lambda(\text{nm}/\text{RIU}) = \Delta\lambda_{\text{peak}}(n_a)/\Delta n_a$ is used [33]. The calculation result shows that, when n_a changes from 1.4 to 1.41, the wavelength sensitivity is up to 4,100 nm/refractive index unit (RIU), which is much higher than that of other PCF SPR sensor coated with ITO film [34]. Finally, In order to calculate the average wavelength sensitivity, the linear fitting between the peak wavelength and n_a is given in Fig. 6(c). The linear regression equation is defined as $\lambda(\mu\text{m}) = 3.2971n_a - 3.1925$. From this equation, we can find that the average wavelength sensitivity of the sensor is 3297.1 nm/RIU when n_a varies from 1.36 to 1.41. Hence, our proposed sensor can be used for cancer cell detection including blood cancer (Jurkat), cervical cancer (HeLa), adrenal glands cancer (PC12), skin cancer (Basal) and so on [35].

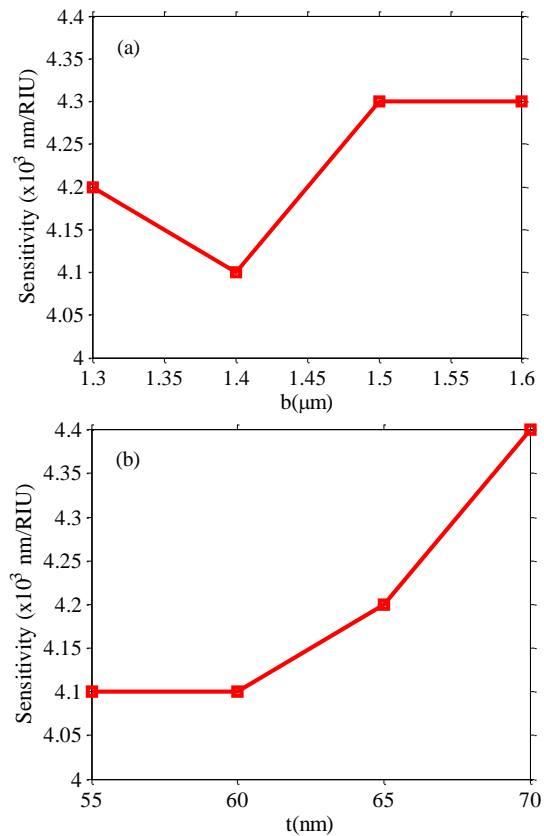


Fig. 7. Influences of fiber parameters b (a) and t (b) on the wavelength sensitivity with n_a increasing from 1.4 to 1.41 (color online)

The effects of fiber parameters b and t on the sensor sensitivity with n_a varying from 1.4 to 1.41 are given in Fig. 7. According to Fig. 7(a), the wavelength sensitivity decreases from 4,200 nm/RIU to 4,100 nm/RIU when b increases from 1.3 μm to 1.4 μm . But if b changes from 1.4 μm to 1.5 μm , the sensor sensitivity increases to 4,300 nm/RIU, and further increasing b to 1.6 μm , the sensor sensitivity keeps unchanged. Fig. 7(b) gives the sensor sensitivity dependence on t . One can observe that the wavelength sensitivity is up to 4,400 nm/RIU when $t = 70$ nm. Assuming a detectable wavelength of 0.01 nm, the detectable index resolution is up to 2.27×10^{-6} . Therefore, our proposed sensor will be useful in various applications including environmentally, food safety, and (bio)chemical detection.

Finally, because our work is purely theoretical, the fabrication possibilities should be solved. The fabrication technology of elliptical air-hole PCF has attracted substantial attention since the elliptical air-hole PCF was first fabricated by Issa et al in 2004 [36]. For instance, Atakaramians et al. declared that elliptical air-hole PCF can be fabricated by employing the existing drawing method including capillary stacking method [37]. Liu et al. draw the elliptical air holes by adopting the ethyl methacrylate monomer polymerization technology to fabricate [38]. Furthermore, 3D printing technology can also be used to draw the elliptical air holes [39]. Therefore, our proposed elliptical air-hole PCF can be fabricated by employing exiting fiber fabrication techniques. After doing that, we can adopt the high-pressure chemical vapor deposition method to deposit ITO layer and infiltrate the channel hole located in the center of fiber core region with analyte, and then, the proposed SPR sensor should be fabricated.

4. Conclusion

In conclusion, a new type of birefringent multi-core PCF SPR sensor coated with ITO layer is proposed. The coupling resonance property and wavelength sensitivity with different fiber parameters are investigated by employing the full vector finite element method. The simulation results indicate that our proposed sensor can be worked in the near-infrared region owing to its several excellent optical properties of ITO. When n_a changes from 1.4 to 1.41, the wavelength sensitivity is 4,400 nm/RIU and the detectable index resolution is up to 2.27×10^{-6} , which is much higher than that of other multi-core PCF SPR sensor [40]. Moreover, the resonance wavelength of the proposed sensor is insensitive to the variations of a and b . This property enhances the tolerance on the sensor drawing defects and fluctuations, and makes our proposed SPR sensor much easier to fabricate.

Acknowledgements

Project supported by the National Natural Science Foundation of China (Grand No.61765003), the Natural Science Foundation of Jiangxi Province, China(Grand No.20181BAB202029), and the Educational Committee Science Foundation of Jiangxi Province, China(Grand No.GJJ18075).

References

- [1] Md. M. Rahman, Md. A. Molla, A. K. Paul, Md. A. Based, Md. M. Rana, M. S. Anower, Results Phys. **18**, 103313 (2020).
- [2] A. Nooke, U. Beck, A. Hertwig, A. Krause, H. Krüger, V. Lohse et al., Sens. Actuators B **149**(1), 194 (2010).
- [3] M.-C. Navarrete, N. Díaz-Herrera, A. González-Cano, Ó. Esteban, Sens. Actuators B **190**, 881 (2014).
- [4] A. Rifat, G. Mahdiraji, D. Chow, Y. Shee, R. Ahmed, F. Adikan, Sensors **15**(5), 11499 (2015).
- [5] Z. Fan, S. Li, Q. Liu, G. An, H. Chen, J. Li et al., IEEE Photonics J. **7**(3), 4800809 (2015).
- [6] A. A. Rifat, F. Haider, R. Ahmed, G. A. Mahdiraji, F. R. M. Adikan, A. E. Miroshnichenko, Opt. Lett. **43**(4), 891 (2018).
- [7] P. Bing, S. Huang, J. Sui, H. Wang, Z. Wang, Sensors **18**(7), 2051 (2018).
- [8] J. Lou, T. Cheng, S. Li, X. Zhang, Opt. Fiber Technol. **50**, 206 (2019).
- [9] M. R. Momota, Md. R. Hasan, Opt. Mater. **76**, 287 (2018).
- [10] A. K. Paul, A. K. Sarkar, A. B. R. Rahan, A. Khaleque, IEEE Sens. J. **18**, 5761 (2018).
- [11] S. Jiao, S. Gu, H. Fang, H. Yang, Plasmonics **14**(6), 685 (2019).
- [12] K. Ahmed, B. K. Paul, B. Vasudevan, A. N. Z. Rashed, R. Maheswar, I. S. Amiri, P. Yupapin, Results Phys. **12**, 2021 (2019).
- [13] A. Rifat, G. Mahdiraji, D. Chow, Y. Shee, R. Ahmed, F. Adikan, Sensors **15**(5), 11499 (2015).
- [14] J. N. Dash, R. Jha, IEEE Photonics Technol. Lett. **26**(6), 595 (2014).
- [15] Z. Fan, S. Li, Q. Liu, G. An, H. Chen, J. Li et al., IEEE Photonics J. **7**(3), 4800809 (2015).
- [16] F. Wang, Z. Sun, C. Liu, T. Sun, P. K. Chu, Opto-Electron. Rev. **26**(1), 50 (2018).
- [17] X. Chen, L. Xia, C. Li, IEEE Photonics J. **10**(1), 6800709 (2018).
- [18] A. A. Rifat, R. Ahmed, G. A. Mahdiraji, F. R. M. Adikan, IEEE Sensors J. **17**(9), 2776 (2017).
- [19] Md. S. Islam, J. Sultana, A. A. Rifat, R. Ahmed, A. Dinovitser, B. W.-H. Ng, H. Ebendorff-Heidepriem, D. Abbott, Optics Express **26**(23), 30347 (2018).
- [20] V. Kaur, S. Singh, Proceedings of the Future Technologies Conference (FTC), 841 (2018).

- [21] T. Huang, *Plasmonics* **12**(3), 583 (2017).
- [22] A. K. Paul, *OSA Continuum* **3**(8), 2253 (2020).
- [23] A. K. Paul, Md. S. Habib, N. H. Hai, S. M. A. Razzak, *Opt. Commun.* **464**, 125556 (2020).
- [24] T. Ahmed, A. K. Paul, Md. S. Anower, S. M. A. Razzak, *Appl. Optics* **58**(31), 8416 (2019).
- [25] A. Boltasseva, H. A. Atwater, *Science* **331**(6015), 290 (2011).
- [26] H. W. Lee, G. Papadakis, S. P. Burgos, K. Chander, A. Kriesch, R. Pala, U. Peschel, H. A. Atwater, *Nano. Lett.* **14**(11), 6463 (2014).
- [27] A. Capretti, Y. Wang, N. Engheta, L. D. Negro, *Opt. Lett.* **40**(7), 1500 (2015).
- [28] C. Rhodes, M. Cerruti, A. Efremenko, M. Losego, D. E. Aspnes, J. P. Maria, S. Franzen, *J. Appl. Phys.* **103**(9), 093108 (2008).
- [29] J. W. Fleming, *Appl. Opt.* **23**(24), 4486 (1984).
- [30] A. Solieman, M. A. Aegerter, *Thin Solid Films* **502**, 205 (2006).
- [31] M. R. Hasan, S. Akter, A. A. Rifat, S. Rana, S. Ali, *Photonics* **4**(4), 18 (2017).
- [32] Z. Tan, X. Hao, Y. Shao, Y. Chen, X. Li, P. Fan, *Opt. Express* **22**(12), 15049 (2014).
- [33] A. A. Rifat, G. A. Mahdiraji, D. M. Chow, Y. G. Shee, R. Ahmed, F. R. Adikan, *Sensors* **15**(5), 11499 (2015).
- [34] J. N. Dash, R. Jha, *IEEE Photonics Technol. Lett.* **26**(6), 595 (2014).
- [35] M. A. Jabin, K. Ahmed, M. J. Rana et al. *IEEE Photonics J.* **99**, 1 (2019).
- [36] N. A. Issa, M. A. V. Eijkelenborg, M. Fellow, F. Cox, G. Henry, M. C. J. Large, *Opt. Lett.* **29**(12), 1336 (2004).
- [37] S. Asaduzzaman, K. Ahmed, *Sens. Bio-Sens. Res.* **10**, 20 (2016).
- [38] F. Liu, H. Gao, Q. Xu, Y. Zhang, *Adv. Mater. Res.* **279**, 151 (2011).
- [39] X. Jiang, N. Y. Joly, R. Sopalla, F. Babic, J. Huang, P. Russell, in *Advanced Photonics 2016 (IPR, NOMA, Sensors, Networks, SPPCom, SOF)*, OSA Technical Digest (online) (Optical Society of America, paper SoW3G1 (2016).
- [40] K. Tong, F. Wang, M. Wang, P. Dang, Y. Wang, *Opt. Fiber Technol.* **46**, 306 (2018).

*Corresponding author: jfliao@126.com